BIOCHEMISTRY
including biophysical chemistry & molecular biology
Article

Biochemistry **2010,** *49,* 6635–6645 6635
DOI: 10.1021/bi100685k

The Response of *Escherichia coli* NikR to Nickel: A Second Nickel-Binding Site[†]

Sheila C. Wang,[‡] Yanjie Li, ManYing Ho, Maria-Elena Bernal, Andrew M. Sydor, Wasim R. Kagzi, and Deborah B. Zamble*

Department of Chemistry, University of Toronto, Toronto, Ontario, Canada M5S 3H6. [‡]*Current address: Chemistry Research Laboratory, University of Oxford, Oxford, United Kingdon OX1 3TA*

Received May 3, 2010; Revised Manuscript Received June 21, 2010

ABSTRACT: The *Escherichia coli* transcription factor NikR mediates two levels of regulatory control of Ni(II) uptake in response to changes in the levels of available nickel. Despite the evidence that metal binding to two distinct sites on NikR, referred to as the high- and low-affinity Ni(II) sites, is required for Ni(II)-selective DNA binding by the protein, the role of the latter set of Ni(II) ions in the activation of NikR remains controversial, and the position of the putative low-affinity Ni(II)-binding site(s) on NikR has not been determined. In this study we confirm that NikR has a high-affinity Ni(II)-binding site that is maintained upon DNA binding. The ligands of the low-affinity Ni(II)-binding site were examined by using selective chemical modification and mass spectrometry performed in the presence of excess Ni(II) and DNA. We localized this Ni(II) site to a region at the interface between the metal- and DNA-binding domains and identified His48 and His110 as residues that participate in the low-affinity Ni(II)-binding response. Mutation of His48 and His110 to asparagines reduces significantly both NikR's tendency to precipitate in the presence of excess Ni(II) and the affinity of the DNA-bound complex in the presence of excess Ni(II). A complete scheme involving all of the metal-binding sites that contribute to the regulatory function of *E. coli* NikR in nickel homeostasis is described.

Bacteria have evolved complex biological mechanisms that regulate the intracellular concentrations of metal ions in order to survive (*1*−*4*). In *Escherichia coli*, one of the principle mechanisms of nickel homeostasis is the tight control of expression of a nickel importer by the nickel-responsive transcriptional regulator NikR (*5*−*7*). NikR is the only metal-responsive member of the ribbon−helix−helix (RHH)[1] family of DNA-binding proteins (*8*−*10*), and it controls transcription of the *nik* operon, which encodes an ABC-type nickel uptake transporter (*11*). In response to an increase in intracellular concentrations of Ni(II), NikR binds to the *nik* operator/promoter and represses transcription of the *nik* operon, thus turning off Ni(II) import (*5*, *12*, *13*).

NikR binds stoichiometric Ni(II) in a square planar coordination geometry (Figure 1) involving three histidines (His87 and His89 from one monomer, His76′ from an opposing monomer) and a cysteine residue (Cys95) (*14*) with an estimated picomolar affinity (*15*, *16*), although weaker affinities have been reported (*17*). These high-affinity Ni(II) sites bridge two DNA-binding dimers, and holo-NikR binds to the DNA as a tetramer (*18*, *19*). The X-ray crystal structure of *E. coli* holo-NikR bound to the *nik* recognition sequence revealed that NikR interacts with the DNA sequence through a combination of specific and nonspecific contacts from the two flanking RHH DNA-binding domains as well as nonspecific contacts from the central metal-binding domains (Figure 1) (*19*). How stoichiometric nickel binding activates DNA binding by NikR is not completely understood, but it is likely that the mechanism involves organization of stable structures in the metal-binding domains (*19*−*21*).

The presence of additional Ni(II)-binding site(s) on *E. coli* NikR is suggested by the observation that the DNA-binding affinity of the protein in the presence of excess nickel is 3 orders of magnitude tighter compared to the protein loaded with stoichiometric Ni(II) (4 metal ions per protein tetramer, referred to as holo-NikR) (*12*, *15*, *18*). Previous experiments also demonstrated that the tight DNA-binding complex induced by excess metal is selective for Ni(II) (*18*), and an indirect measurement was used to estimate an affinity of 30 nM for Ni(II) binding to this second type of site (*18*), which is often referred to as the "low-affinity site". Given an intracellular NikR concentration of 200 nM (*15*) and that a few "free" Ni(II) ions per cell translate into a nanomolar concentration (*22*), this low-affinity Ni(II) site is likely physiologically relevant. The model that there are two Ni(II)-binding sites on NikR that modulate two levels of regulatory control is supported by an *in vivo* reporter assay that demonstrated that *E. coli* NikR mediates a basal level of repression on the *nik* promoter under low Ni(II) conditions and complete repression at higher concentrations of added Ni(II) (*13*).

The location of the low-affinity Ni(II)-binding site on *E. coli* NikR and the mechanism by which it modulates DNA binding are not known. The structure of the DNA complex of NikR loaded with stoichiometric nickel revealed two additional metal ions at the interface of the DNA-binding and metal-binding domains which were modeled as potassium cations (Figure 1) (*19*). In the structure of a NikR homologue from *Pyrococcus horikoshii*

[†]This work was supported in part by funding from the Natural Sciences and Engineering Research Council (Canada), the Canadian Institutes of Health Research, and the Canada Research Chairs program.

*To whom correspondence should be addressed. Phone/Fax: (416) 978-3568. E-mail: dzamble@chem.utoronto.ca.

[1]Abbreviations: DTNB, 5,5′-dithiobis(2-nitrobenzoic acid); DTT, dithiothreitol; *E. coli*, *Escherichia coli*; EDTA, ethylenediaminetetraacetic acid (disodium salt); EGTA, ethylene glycol bis(1-aminoethyl ether)-*N*,*N*,*N*′,*N*′-tetraacetic acid; MS, mass spectrometry; MSA, mobility-shift assay; PAR, 4-(2-pyridylazo)resorcinol; RHH, ribbon−helix−helix; SDS−PAGE, sodium dodecyl sulfate−polyacrylamide gel electrophoresis; Tris, tris(hydroxymethyl)aminomethane; XAS, X-ray absorption spectroscopy.

Published on Web 06/28/2010

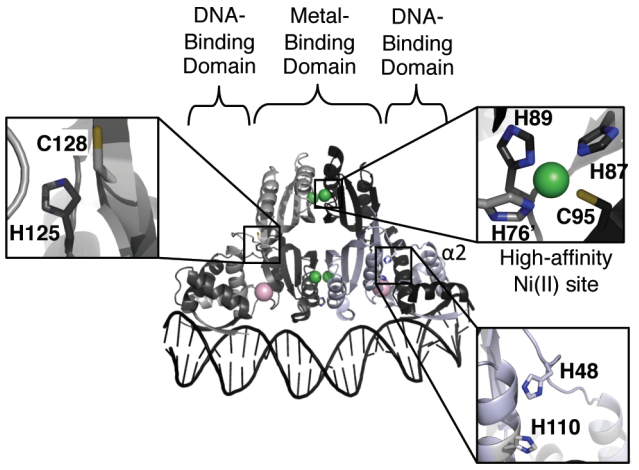

FIGURE 1: *E. coli* holo-NikR DNA complex. The operator-bound NikR tetramer (PDB ID: 2HZV) is drawn with each monomer in a different shade of gray. Two ribbon−helix−helix DNA-binding domains flank the tetrameric core of four metal-binding domains. The high-affinity Ni(II) ions are colored in green and are coordinated by H87, H89, and C95 of one monomer and H76′ of the opposing monomer (shown in inset). The potassium ions are colored in pink. Candidate residues of the low-affinity Ni(II) site are shown in insets. The α2 helix is labeled on one monomer.

(*P. horikoshii*) solved in the absence of DNA, Ni(II) ions were modeled into similar sites (*23*), suggesting that the potassium ions were acting as placeholders for the low-affinity nickel ions. However, biochemical experiments revealed that K^+ is required for DNA binding by *E. coli* NikR even in the presence of just stoichiometric Ni(II) (*24*), and computational analysis suggests that potassium binding is more favorable at this site than nickel (*20*). Furthermore, the only structural information to date about the low-affinity Ni(II) site comes from X-ray absorption spectroscopy (XAS) studies of NikR with Cu(II) and Ni(II) loaded in the high- and low-affinity sites, respectively, which revealed that the Ni(II) ion is coordinated to six N/O donors including two imidazoles (*25*), an environment distinct from the O_6 coordination sphere of the potassium sites (*19*).

Additional secondary nickel sites have been observed in crystal structures of NikR homologues (*23*, *26*). For example, the crystal structure of *Helicobacter pylori* NikR revealed external nickel-binding sites at the surface of the tetramerization interface of the protein (*26*), and a recent study demonstrated that these external sites are important for DNA binding to some promoters (*27*). However, other biochemical results demonstrated that *H. pylori* NikR does not seem to respond to more than stoichiometric nickel binding (*28*−*33*), which suggests that the low-affinity Ni(II)-induced DNA-binding response of *E. coli* NikR is not conserved in all NikR orthologues.

The aim of this study was to resolve some of the discussion in the literature with regard to the distinct nickel-binding sites of *E. coli* NikR and to identify residues that contribute to the elusive low-affinity Ni(II) site. First we address an alternative explanation for the apparent increase in DNA-binding affinity in the presence of extra metal, which is that there is only one metal-binding site on NikR but the metal site changes upon DNA binding. The results confirm that the high-affinity Ni(II) site is preserved upon DNA binding, consistent with the crystal structures of the Ni(II)−NikR−DNA complex and some spectroscopy (*19*, *25*), and support the hypothesis that the tighter DNA-binding response observed in the presence of excess metal is activated by filling low-affinity site(s) on *E. coli* NikR. To locate this Ni(II) site, we applied a combination of chemical modification and mass spectrometry (MS), and the results of these experiments were confirmed by the analysis of corresponding NikR mutants. The results presented here support the model that NikR harbors two distinct Ni(II)-binding sites that regulate two levels of DNA binding. Possible functions of the different metal-binding sites in the activation of *E. coli* NikR are discussed.

MATERIALS AND METHODS

Materials. Restriction endonucleases, kinases, and polymerases were obtained from New England Biolabs. DNA oligonucleotides were purchased from Integrated DNA Technologies. The concentrations of metal stock solutions were confirmed by inductively coupled plasma-atomic emission spectroscopy (ICP-AES). All other reagents were of molecular biology grade from Sigma except where noted. The plasmids pNIK103 and pPC163 were generously donated by P. Chivers (Washington University School of Medicine, St. Louis, MO) (*12*). All of the samples were prepared with Milli-Q water, 18.2 MΩ-cm resistance (Millipore), and the pH of all Tris buffers was adjusted with HCl at room temperature.

Mutagenesis and Protein Purification. The NikR mutants were constructed from the pNIK103 parent plasmid (*12*) by using the QuikChange PCR mutagenesis method (Stratagene) with the primers listed in Table S1. The fidelity of the mutagenesis was confirmed by DNA sequencing (ACGT, Toronto). Both wild-type NikR and mutant proteins were purified on a Ni(II)-NTA column (Qiagen, Valencia, CA), followed by anion exchange on a MonoQ HR10/10 FPLC column (GE Healthcare), as described previously (*12*, *16*). Apo-NikR was generated by incubating NikR with 1 mM EDTA and 1 mM DTT at 4 °C overnight after the first chromatography step, and EDTA and DTT were removed in the second anion-exchange step. The lack of metal in the apo form of the protein was confirmed by the absence of an absorbance signal at 302 nm and by ICP-AES.

The molecular masses of wild-type NikR and mutants were confirmed by electrospray ionization mass spectrometry (ESI-MS; Department of Chemistry, University of Toronto) ($M_{r\text{-}calc}$ NikR = 15093.7 Da, $M_{r\text{-}obs}$ NikR = 15094.0 Da, $M_{r\text{-}calc}$ H48N = 15070.4 Da, $M_{r\text{-}obs}$ H48N = 15070.0 Da, $M_{r\text{-}calc}$ H92A = 15027.3 Da, $M_{r\text{-}obs}$ H92A = 15028.0 Da, $M_{r\text{-}calc}$ H110N = 15070.4 Da, $M_{r\text{-}obs}$ H110N = 15070.0 Da, $M_{r\text{-}calc}$ H48/110N = 15046.3 Da, $M_{r\text{-}obs}$ H48/110N = 15046.0 Da, $M_{r\text{-}calc}$ H125N = 15070.4 Da, $M_{r\text{-}obs}$ H125N = 15070.0 Da, $M_{r\text{-}calc}$ C128A = 15061.3 Da, $M_{r\text{-}obs}$ C128A = 15062.0 Da). An assay with 5,5′-dithiobis(2-nitrobenzoic acid) (DTNB) was used to confirm that the proteins were >95% reduced. All protein concentrations are listed in terms of the monomer concentration.

Carbamidomethylation of Cysteine Residues in NikR Using Iodoacetamide. Samples of 30−40 μM apo-, Ni(II)-, and excess Ni(II)-NikR (NikR in the presence of 5 equiv of excess Ni(II)) were incubated with 1 equiv of an HPLC-purified 54-bp DNA fragment from the *nik* promoter that contains the NikR recognition sequence (Table S1) for 1 h at room temperature in 20 mM Tris-HCl buffer at pH 7.6, 100 mM KCl, and 3 mM $MgCl_2$ followed by modification with a 50-fold molar excess of iodoacetamide for 20 min at room temperature in the dark. The reactions were quenched by adding a 50-fold molar excess of dithiothreitol with respect to the protein concentration, and then the protein was buffer exchanged into 20 mM Tris, pH 7.6, by gel filtration on a PD-10 column (GE Healthcare). Samples were

submitted immediately for analysis by ESI-MS. Experiments with apo- and Ni(II)-bound NikR in the absence of DNA were performed under the same conditions.

Carbethoxylation of Histidine Residues in NikR Using Diethyl Pyrocarbonate. Samples of 30−40 μM apo-, Ni(II)-, and excess Ni(II)-NikR were incubated with 1 equiv of the 54-bp DNA fragment from the *nik* promoter for 1 h in 20 mM Tris-HCl buffer at pH 7.6, 100 mM KCl, and 3 mM $MgCl_2$ at room temperature and then modified with a 50-fold molar excess of diethyl pyrocarbonate (DEPC) for 5 min at room temperature in the dark. The modification reaction has been shown to be specific for histidine residues between pH 5.5 and pH 7.5 (*34*). The reaction was quenched by the addition of a 50-fold molar excess of imidazole, and then the buffer was exchanged into 20 mM Tris, pH 7.6, by gel filtration on a PD-10 column. Samples were submitted immediately for analysis by ESI-MS. Experiments with apo- and Ni(II)-bound NikR in the absence of DNA were performed under the same conditions except that half as much DEPC was used.

ESI-MS of the Chemically Modified Proteins. ESI-MS was performed using a Sciex QStar quadrupole-time-of-flight (QToF) mass spectrometer equipped with a TurboIonSpray electrospray source. Calibration was performed with a mixture of CsI, verapamil, and the peptide ALILTLVS. Data precision was estimated by taking 18 measurements of apomyoglobin after calibration of the mass scale with the ALILTLVS peptide at m/z 829. These measurements were reconstructed without smoothing, and the reconstructed masses were analyzed giving a median MW of 16951.48 units for the protein and an average absolute deviation from the median of 0.137 unit. For small ions (< 1000 units) a 5 ppm mass accuracy or better was routinely achieved. Protein and peptide mass spectra were analyzed by using the BioAnalyst 1.15 software package (Applied Biosystems/MDS Sciex). The ion spray voltage was set at 5.5 kV and a declustering potential of 65 V applied. A TurboIonSpray drying gas (N_2) temperature of 300 °C was employed. Sample volumes of ∼2 μL were injected into a 10 μL loop, and an Agilent 1100 LC was used to infuse the sample through a refillable desalting column (Tricorn, 5 mm diameter, 50 mm length; Sephadex G25-80, Sigma) at a flow rate of 250 μL/min. The mobile phase was H_2O/methanol (1:1) with 0.1% formic acid to assist protonation. The mass spectrometer was operated in the positive ToF RF only mode, and ions were collected over the m/z range of 400−1500.

Tryptic Digestion of Chemically Modified NikR Derivatives. Chemically modified NikR−DNA complexes were preincubated with 10 mM EDTA for 1 h to disrupt NikR−DNA binding, and then the buffer was exchanged into 20 mM Tris, pH 7.6, by gel filtration on a PD-10 column. Aliquots of 30 μL of chemically modified NikR derivatives were digested with 20 μL of trypsin solution (1 μg/μL, Promega trypsin gold, mass spectrometry grade) in 20 mM Tris, pH 7.6, 100 mM KCl, and 5 mM $CaCl_2$. After 3 h of incubation at 37 °C, aliquots were taken for immediate matrix-assisted laser desorption/ionization (MALDI) MS analysis.

MALDI MS Analyses. MALDI-time-of-flight mass spectrometry (MALDI-TOF-MS) analyses were performed using a Waters Micromass MALDI micro MX mass time-of-flight spectrometer equipped with a UV-nitrogen laser (337 nm) and a microchannel plate detector. The molecular weight determination acceleration voltage was set to 25 kV. For peptide mapping experiments the acceleration voltage was set to 10 kV. Protein- or peptide-containing solution (1 μL) was mixed with 1 μL of matrix solution (10 μg/μL 4-hydroxy-α-cyanocinnamic acid dissolved in acetonitrile/0.1% trifluoroacetic acid (2:1)) directly on the target. MALDI MS/MS data were obtained from the Hospital For Sick Children (Toronto, Ontario).

Quaternary Structure Analysis. The quaternary structures of holo-NikR, wild type and mutants, were analyzed by size exclusion chromatography on a Superdex S-200 gel filtration column (GE Healthcare) equilibrated in 25 mM HEPES, pH 7.5, and 100 mM KCl.

Circular Dichroism. CD spectra were recorded on a Jasco model J-810 spectropolarimeter at room temperature. The protein concentrations ranged from 10 to 15 μM in 20 mM Tris, pH 7.6, and 100 mM KCl. Each CD spectrum was the average of five accumulations and normalized to mean residue ellipticity [θ] (deg cm^2 $dmol^{-1}$) using the equation $[\theta] = (\theta \times 100)/(nlc)$, where n is the number of residues, c is the total protein concentration (millimolar), l is the cell path length, and θ is the measured ellipticity (millidegrees).

Metal Binding. Electronic absorption spectra were routinely collected at 25 °C on an Agilent 8453 spectrophotometer equipped with an 89090A Peltier temperature controller. Ni(II)-titration experiments with NikR were performed in 20 mM Tris, pH 7.6, 100 mM KCl, and Ni(II) concentrations as noted. EGTA competition experiments were performed with separate aliquots of protein incubated overnight at room temperature. Samples containing 10 μM NikR or mutant proteins in 20 mM Tris, pH 7.6, and 100 mM KCl were incubated with 10 mM EGTA and increasing concentrations of Ni(II). The fraction of Ni(II)−NikR was calculated by using the extinction coefficient measured with a nickel titration in the absence of competitor, and the concentration of free nickel was calculated as described previously (*16*). The data were fit to a Langmuir equation with a variable Hill coefficient n, $r = [Me]^n/((K_{d(app)})^n + [Me]^n)$, where r is the fraction of protein bound to metal and $K_{d(app)}$ is the concentration of free metal required for 50% binding.

DNase Footprinting. DNase footprinting assays were performed with a 133-bp DNA probe containing the *nik* promoter (*18*). The DNase footprinting reactions were carried out in 20 mM Tris, pH 7.5, 100 mM KCl, 1 mM $MgCl_2$, 5% (v/v) glycerol, and 100−300 pM ^{32}P-labeled probe (∼30000−80000 cpm/sample). Metal salts and NikR were added as noted. The DNase footprinting gels were vacuum-dried, exposed to a phosphor screen, scanned on a Molecular Dynamics Storm 860 phosphorimager, and analyzed with ImageQuant 5.0 software. Each lane was normalized to account for sample loading, and the degree of protection was determined by quantitation of the intensity of two bands within the binding sequence. Half-maximal binding was calculated by fitting the data to a Langmuir equation with a variable Hill coefficient n, $r = [NikR]^n/((K_{d(app)})^n + [NikR]^n)$, where r is the fraction of DNA bound to NikR and $K_{d(app)}$ is the concentration of protein required for 50% binding (*18*). The numbers reported are the averages and standard deviations from the fits of at least triplicate experiments.

Mobility-Shift Assays. Electrophoretic mobility-shift assays (MSAs) were performed with the same 133-bp DNA fragment used in DNase footprinting experiments described above. The indicated concentrations of protein were loaded with stoichiometric nickel and incubated with the DNA in a binding buffer containing 20 mM Tris, pH 7.6, 100 mM KCl, 3 mM $MgCl_2$, 0.1% IGEPAl, 5% glycerol, and 0.1 mg/mL sonicated herring sperm DNA (Promega, Madison, WI). Excess nickel was added to the binding buffer, running buffer, and the 7% native

polyacrylamide gel before polymerization to a final concentration of 35 μM. The gels were run at 300 V and 4 °C, vacuum-dried, and then analyzed on the phosphorimager. Half-maximal binding was calculated by fitting the data as described for the DNase footprinting assays.

Metal Release. NikR (10 μM) loaded with 0.9 equiv of nickel sulfate was incubated with or without 2.5 μM 54-bp oligonucleotide for 2 h at room temperature in MSA binding buffer. Following the addition of 50 μM 4-(2-pyridylazo)-resorcinol (PAR), metal release from NikR was detected by monitoring the formation of the 2:1 PAR−nickel complex at 500 nm (*35*, *36*) over the course of 8 h with the absorption measured every 2 min. The concentration of the PAR_2−Ni(II) complex was determined from a standard curve prepared with nickel sulfate under the same conditions. The total amout of nickel in the sample was confirmed by adding *p*-hydroxymercuribenzoic acid to the protein in the presence of PAR.

X-ray Absorption Spectroscopy. The Ni(II)−NikR XAS sample was prepared by incubating ~250 μM NikR in buffer containing 100 mM KCl and 3 mM $MgCl_2$ with 0.9 equiv of Ni(II) overnight at room temperature and then concentrating the protein to ~500 μM. Ni(II) binding was confirmed by electronic absorption spectroscopy at 302 nm with a calculated extinction coefficient of 7200 M^{-1} cm^{-1}. The DNA-bound Ni(II)−NikR XAS sample was prepared by incubating ~250 μM NikR with 0.9 equiv of Ni(II) and 1 equiv of the 54-bp oligonucleotide per tetramer overnight at room temperature. The samples were then concentrated in 20% glycerol (in water) to a final concentration of ~1 mM. Both samples were subsequently frozen with liquid nitrogen and stored at −80 °C before being transferred and frozen with liquid nitrogen in (2 × 10 × 10 mm) Lucite sample cuvettes for data acquisition. XAS measurements were carried out at the Stanford Synchrotron Radiation Laboratory (SSRL), and nickel K-edge data were collected on the structural molecular biology beamline 9-3 as previously described (*37*). For each sample three to six scans were accumulated, and the energy was calibrated by reference to the absorption of a nickel metal foil measured simultaneously with each scan, assuming a lowest energy inflection point of 8331.6 eV for Ni(II). XAS analyses were carried out as described previously (*37*). The formation of a NikR−DNA complex with this oligonucleotide was confirmed by using MSA experiments with the same preparations of protein and oligonucleotide.

RESULTS

The Role of Excess Ni(II) Ions in the Activation of NikR. Whether or not a low-affinity Ni(II) site exists and the role of excess Ni(II) ions in the activation of NikR are subjects of discussion (*17*, *38*). Another possible explanation for the apparent increase in the DNA-binding affinity of NikR in the presence of extra Ni(II) is that there is only one Ni(II)-binding site on the protein but that the coordination structure changes upon DNA binding, resulting in a weaker Ni(II) affinity. This hypothesis is supported by an XAS study that revealed a dramatic change in the nickel coordination sphere of the holoprotein, from four- to six-coordinate accompanied by loss of the thiolate ligand, upon addition of DNA oligonucleotides containing the *nik* recognition sequence (*39*). However, a change in the high-affinity site is not consistent with the crystal structures of the nickel-bound NikR and nickel-bound NikR-operator complexes in which the square planar coordination site is unaltered (*14*, *19*). Furthermore, in subsequent XAS analysis of NikR performed in the presence of *nik* DNA and excess metal a transformation of the high-affinity nickel site was not observed (*25*).

To examine if the high-affinity Ni(II) coordination site changes upon DNA binding, XAS analyses of holo-NikR in the presence and absence of an oligonclueotide containing the *nik* recognition sequence were performed by our laboratory. XAS of Ni(II)-bound NikR and the Ni(II)-bound NikR operator complex produced nearly identical near-edge spectra, each displaying a $1s\text{-}4p_z$ pre-edge peak at 8334 eV that is typical of square planar Ni(II) complexes (*40*) (Figure S1), and both near-edge spectra resemble that reported previously for the holo complex (*39*). The XAS data collected were of insufficient quality to perform EXAFS analyses as well. However, these experiments confirm that the high-affinity Ni(II) coordination site is maintained upon addition of DNA. In order to determine if the high-affinity site is weakened upon DNA binding, a metal release assay was employed. In this experiment, as nickel comes off NikR over time, it is captured by the metallochromic indicator PAR, and we have previously used this assay to monitor the slow nickel release from the subpicomolar affinity nickel site in *E. coli* HypB (*36*). When NikR is incubated with PAR, only approximately half of the nickel bound to the protein is released into solution over the course of 7 h (Figure S2). The addition of the oligonucleotide containing the NikR recognition sequence did not accelerate loss of metal from the protein. Although this experiment does not measure the affinity of stoichiometric nickel binding to NikR, it does suggest that the strength of the high-affinity nickel-binding site is not compromised significantly upon DNA binding.

Reactivities of Cysteines: Modification of NikR with Iodoacetamide and Localization of Cysteines Involved in Ni(II) Binding. Direct observation of metal binding to the low-affinity Ni(II) site of *E. coli* NikR is hindered by the fact that at the concentrations required for spectroscopic absorption experiments the protein precipitates when exposed to excess metal. The presence of a DNA oligonucleotide containing the *nik* recognition sequence stabilizes the protein, but the intense DNA absorption precludes using electronic absorption spectroscopy to obtain information about the low-affinity Ni(II) site. To identify residues in *E. coli* NikR of potential significance to the binding of nickel, we used a combination of chemical modification and mass spectrometry. Metal binding to nucleophilic side chains can block covalent modifications (*41*, *42*), and a comparison of the MS of reactions performed in the presence and absence of metal reveals the number of the targeted residues that serve as metal-binding ligands. Subsequent digestion and MS sequencing can then be used to identify the protected amino acids.

The reactivities of the cysteine residues in the various states of NikR were examined first. Initial experiments to test this approach were performed with NikR loaded with 1:1 Ni(II) because the ligands were identified previously by using several other methods. *E. coli* NikR contains two cysteines at positions 95 and 128, and Cys95 is a ligand in the high-affinity Ni(II) site (*14*, *19*). Upon reaction of thiols with iodoacetamide, carboxamidomethylation results in a mass increase of 57 Da/cysteine (Figure S3), and the extent of modification of NikR under different Ni(II) conditions was determined by ESI-MS. Only the monomeric form of NikR (15094 Da) is observed by ESI-MS under our experimental conditions. Modification of apo-NikR with excess iodoacetamide results in two populations

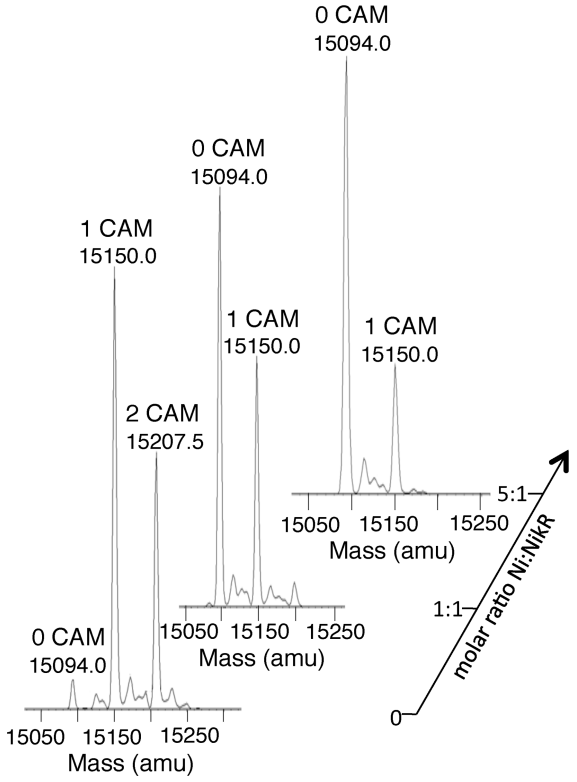

FIGURE 2: ESI mass spectra following the carboxamidomethylation of NikR in the presence of DNA and increasing Ni(II) concentrations. NikR was modified with excess iodoacetamide in the presence of an oligonucleotide containing the *nik* recognition sequence and 0, 1, or 5 equiv of Ni(II). The reactions were quenched with excess DTT and analyzed by ESI MS. Incorporation of one carboxamidomethyl group (CAM) results in a molecular mass increase of 57 Da. The molecular mass of the unmodified NikR monomer is 15094 Da.

of species bearing one or two labels, indicating that both cysteines are susceptible to modification (Figure S4). Incubation of the protein with 1 equiv of Ni(II) prior to derivitization results in two populations consisting of the unmodified protein and a singly labeled species, indicating that one cysteine is protected from modification upon loading the protein with stoichiometric nickel (Figure S4). Subsequent MALDI MS/MS analysis of tryptic fragments identified Cys95 as the protected amino acid (data not shown), consistent with previous structural and biochemical studies (*14*, *19*, *39*). These results demonstrate that Ni(II) coordination to the cysteine in the high-affinity Ni(II) site is strong enough to block the reaction with iodoacetamide and that iodoacetamide modifies cysteines specifically under the experimental conditions used.

The next set of experiments was performed in the presence of an oligonucleotide containing the sequence from the *nik* promoter that is recognized by NikR. NikR was incubated with the DNA and no metal, 1 equiv of Ni(II), or 5 equiv of Ni(II) prior to exposure to excess iodoacetamide. One modification is observed in the presence of either stoichiometric or excess Ni(II) (Figure 2), suggesting that the second cysteine, Cys128, is not involved in low-affinity Ni(II) binding. Furthermore, the observation that one cysteine is still protected in the presence of DNA and 1:1 Ni(II) supports the conclusion that the high-affinity Ni(II) site remains the same even after DNA binding.

The Cysteine Mutant Confirms That C128 Is Not Involved in Low-Affinity Ni(II) Binding. To test the hypothesis that Cys128 is not a ligand of the low-affinity Ni(II) site of NikR,

Table 1: Apparent DNA-Binding Affinities of NikR and Mutants to the *nik* Promoter[a]

	1:1 Ni(II)[b]	excess Ni(II)[c]
WT	33 ± 6	0.010 ± 0.002
C128A	50 ± 10	0.04 ± 0.01
H48N	N/A	>0.1[d]
H92A	N/A	~0.01
H110N	N/A	>0.1[d]
H48/110N	358 ± 29	15 ± 2[e]
H125N	N/A	~0.01

[a]The affinities reported are the concentrations of protein required to reach 50% saturation ($\times 10^{-9}$ M) and represent the average of a minimum of three independent experiments ± standard deviation. [b]Determined by DNase footprinting. [c]Determined by MSA experiments with 35 μM Ni(II) in the gel and running buffer. [d]Estimated with the assumption that ≈10% of the DNA must be shifted to be detected. [e]A similar number was measured in DNase footprinting experiments performed with 35 μM nickel.

Cys128 was mutated to an alanine. Control experiments confirmed that the mutation did not affect either the secondary or quaternary structures (as reported by circular dichroism and size exclusion chromatography, respectively, Figure S5) or the high-affinity Ni(II)-binding properties (as determined by EGTA competition experiments, Figure S6) of NikR. To confirm that the DNA-binding properties of C128A in the presence of stoichiometric Ni(II) are also similar to that of wild-type NikR, DNase footprinting experiments were performed. In the presence of stoichiometric Ni(II) C128A bound to the DNA and produced a footprint in the same location as wild-type NikR (Figure S7), around the *nik* transcription start, with a half-maximal binding affinity of 50 ± 10 nM, a K_D comparable to that of wild-type NikR (Table 1). Picomolar DNA-binding affinities in the presence of excess Ni(II) could not be measured by DNase footprinting, so the affinity of C128A for a DNA probe containing the *nik* operator in the presence of excess Ni(II) was examined by mobility-shift assay (MSA). In the presence of 35 μM excess Ni(II), the K_D for the C128A−DNA complex is 40 ± 10 pM (Figure 3 and Table 1), a DNA-binding affinity only several-fold weaker than that of wild-type NikR. These experiments support the conclusion that C128 is not a ligand of the low-affinity Ni(II) site of NikR and that this residue does not make a significant contribution to Ni(II)-responsive DNA binding.

Reactivities of Histidines: Modification of NikR with DEPC and Localization of Histidines Involved in Ni(II) Binding. *E. coli* NikR contains 12 histidines per monomer, and diethyl pyrocarbonate (DEPC) was used to probe the differential reactivities of the histidine side chains in apo- and Ni(II)-NikR. DEPC reacts with the imidazole group to yield a carbethoxylated product (Figure S3). The addition of one carbethoxy group produces a mass increase of 72 Da, but unlike other nucleophilic side chains, the histidine can be modified twice (*43*). Mass analyses of DEPC-treated apo- and Ni(II)-NikR revealed up to 14 and 11 modifications, respectively, suggesting that at least two of the histidines in apo-NikR have been modified twice (Figure S8). The largest peak amplitudes of DEPC-treated apo- and Ni(II)-NikR correspond to 11 and 8 modifications, respectively (Figure S8). The relative mass difference of three carbethoxy groups between the apo- and Ni(II)-loaded forms of NikR is consistent with the roles of His76, His87, and His89 as high-affinity Ni(II)-binding ligands. Subsequent MALDI MS analyses of tryptic peptides of DEPC-modified apo- and Ni(II)-NikR revealed that only peptides containing histidines were modified. Although other amino acids, such as Ser and Tyr, can also react with excess

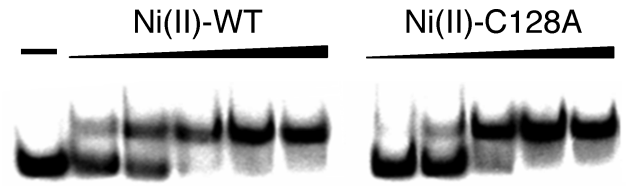

FIGURE 3: DNA binding of wild-type or C128A NikR in the presence of excess nickel. Increasing concentrations of wild-type or mutant C128A NikR (1 pM to 10 nM) were incubated with a radiolabeled 133-bp oligonucleotide containing the *nik* promoter in the presence of 35 μM $NiSO_4$. The reactions were analyzed on a 7% native gel with 35 μM $NiSO_4$ in the gel and running buffer. No protein was added to the first lane.

DEPC (*43*), there was no evidence in the MS/MS analyses of nonspecific modification. All of the protected histidines were localized to the largest tryptic peptide (residues 71−102, ~3600 Da), which includes the three high-affinity Ni(II)-binding histidines (Figure 4B). However, conclusive MS/MS analysis of this peptide was not possible because low peptide ion abundance in the gas phase and low fragmentation efficiency generated MS/MS spectra of insufficient quality to resolve unambiguously the reactivity profiles of five of the seven closely spaced histidines, His77−79, His87, and His89 (see Figure S8 for more detailed discussion). However, MALDI MS/MS analyses confirmed that the first histidine in the tryptic peptide, His76, was protected from DEPC modification by stoichiometric Ni(II) (data not shown) and that the last histidine in the peptide, His92, was not.

To determine if additional histidines are protected from DEPC modification in the presence of excess Ni(II) and DNA, NikR was incubated with an oligonucleotide containing the *nik* promoter and either no metal, 1 equiv of Ni(II), or 5 equiv of Ni(II) prior to exposure to a 50-fold excess of DEPC (Figure 4A). Previous studies have demonstrated that DEPC reacts with nucleic acids (*44*, *45*) so to ensure that the protein was fully derivitized, the concentration of DEPC used in the presence of DNA was increased by 2-fold compared to the experiments performed without DNA described above. The overall extent of derivitization of the whole protein increased in the presence of the higher concentrations of DEPC (compare Figures S8 and 4A); however, the relative mass difference of three carbethoxy groups between the apo- and Ni(II)-loaded forms of NikR was maintained (Figure 4A), consistent with the roles of His76, His87, and His89 as high-affinity Ni(II)-binding ligands.

Although the number of DEPC modifications on NikR seemed to decrease in the presence of excess Ni(II) and DNA, this experiment could not be reliably reproduced because the protein was not consistently observed by MS under these experimental conditions (data not shown). It is possible that the carbethoxylation of multiple ionizable histidine residues combined with the high stability of the NikR−DNA complex formed in the presence of excess Ni(II) reduces the probability of detecting the DEPC-modified protein. It should be noted that the number of histidines protected from chemical modification cannot be determined directly from the mass spectra of the carbethoxylated whole protein in any case because accessible/reactive histidines can be modified twice. Therefore, we proceeded to the next step and performed MALDI MS peptide mapping and MALDI MS/MS of tryptic peptides derived from DEPC-modified NikR under various Ni(II) conditions to identify which histidines were protected from DEPC only in the presence of excess Ni(II).

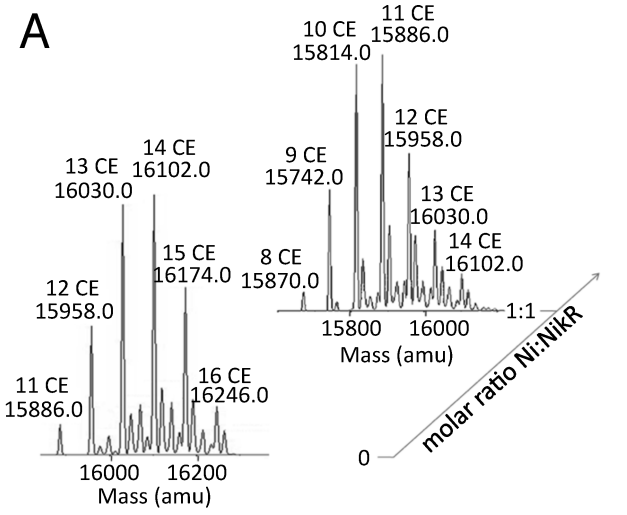

B

1 MQR | **VTITLDDDLLETLDSLSQR** | **RGYNNR** | **SE** 30
31 **AIRDILR** | **SALAQEATQQHGTQGFAVLSYVY** 60
61 **EHEK** | **R** | DLASR | **IVSTQHHHHDLSVATLHVHI** 90
91 **NHDDCLEIAVLK** | **GDMGDVQHFADDVIAQR** | G 120
121 VR | **HGHLQCLPK** | ED

FIGURE 4: Carbethoxylation of NikR in the presence of DNA and increasing Ni(II) concentrations. (A) NikR was modified with excess DEPC in the presence of an oligonucleotide containing the *nik* promoter and 0 or 1 equiv of Ni(II). The complex formed in the presence of 5 equiv of metal and DNA was not detected consistently by MS. The reactions were quenched with excess imidazole and analyzed by ESI MS. Incorporation of one carbethoxy group (CE) results in a molecular mass increase of 72 Da. Histidine imidazole groups can be modified by DEPC also at the second nitrogen atom (bis-modification). The molecular mass of the unmodified NikR monomer is 15094 Da. (B) The primary sequence of NikR. The tryptic fragments of the apo-, Ni(II)-, and excess Ni(II)−NikR−DNA complexes observed in the MS analyses are shown in bold.

Peptide assignment covered 90% of the sequence (Figure 4B), and peptides without histidines were not modified (data not shown) in the presence of DNA under any of the conditions used. Expanded views of the regions of the MALDI mass spectra of tryptic peptides containing histidines are shown in Figure 5. The spectra revealed that peptides containing His110 (Figure 5A), His48, and His62 (Figure 5B) and His76−79, His87, His89, and His92 (Figure 5C) have at least one histidine that was shielded from carbethoxylation by the presence of excess Ni(II). In contrast, although there is a slight change in modification pattern of the peptide containing His123 and His125, no clear protection of histidines was observed in the presence of excess Ni(II) (Figure 5D), which was later confirmed by MS/MS.

MS/MS analyses of the peptide fragments identified His48 and His110 as residues that are selectively protected from DEPC modification in the presence of excess Ni(II). A representative example of fine mapping of DEPC modification sites by MS/MS analyses is presented in Figure S9. MS/MS sequencing of the monocarbethoxylated peptide containing residues 38−65 (thus encompassing His48 and His62) obtained from DEPC reactions performed in the presence of stoichiometric and excess Ni(II) is nearly complete (Figure S9). A listing of b- and y-type fragment ions is presented in Figure S9A. Carbethoxylated b_{11-24} (which includes His48 only) and carbethoxylated y_{4-17}

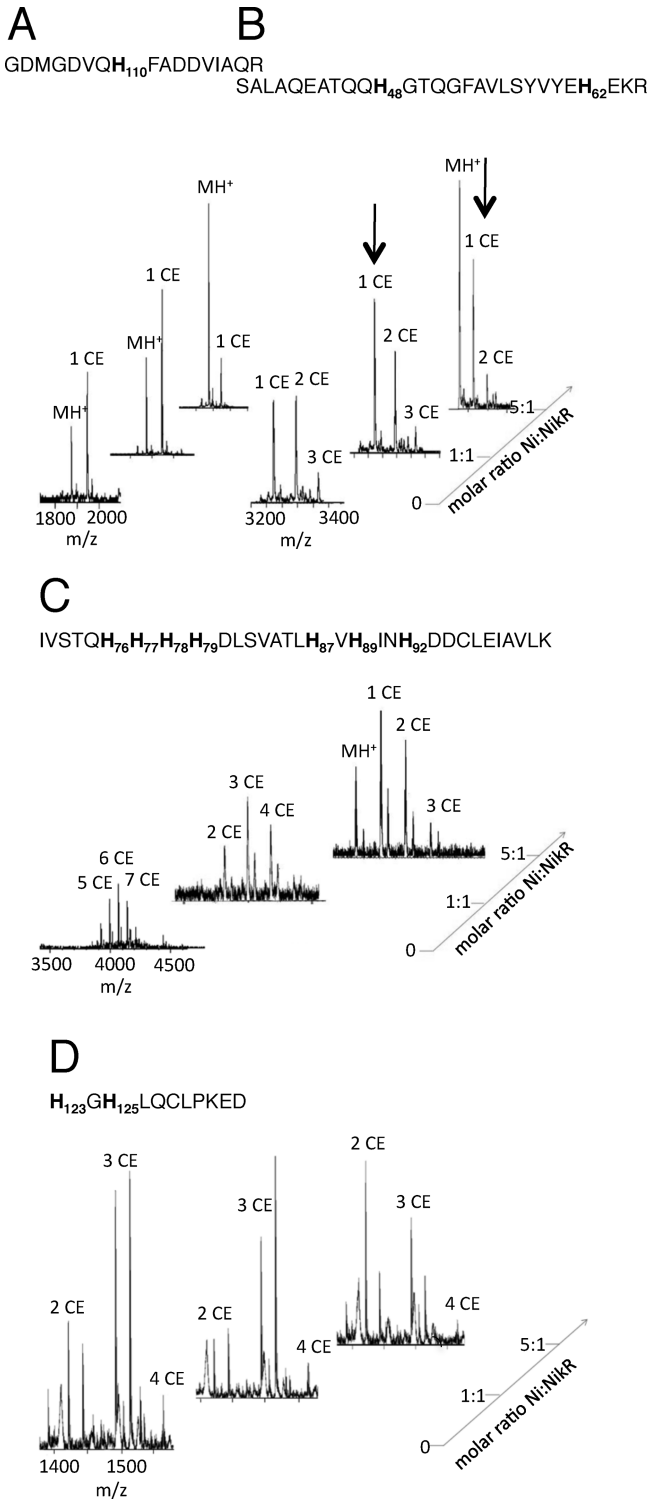

FIGURE 5: MALDI MS peptide mapping analyses of NikR and DEPC-modified derivatives. MALDI MS spectra of tryptic peptides of DEPC-modified apo-, Ni(II)-, and excess Ni(II)−NikR containing residues 103−119 (A), 38−65 (B), 71−102 (C), and 123−133 (D). The unmodified singly charged (MH^+) ions are shown. Incorporation of one carbethoxy group (CE) yields a molecular mass increase of 72 Da. In some cases a sodium adduct is also observed. The MS/MS data of the peptides indicated by arrows in (B) are shown in detail in Figure S9.

(which includes His62 only) fragment ions were both detected in the singly modified peptide obtained following DEPC modification of the Ni(II)−NikR−DNA complex (Figures S9B), suggesting that both His48 and His62 are equally susceptible to chemical modification in the presence of 1:1 Ni(II) and DNA. In contrast, unmodified/bare b fragment ions and modified y fragment ions were detected predominantly in the singly modified peptide obtained from the NikR−DNA complex modified in the presence of excess Ni(II) (Figure S9C), demonstrating that His48 is protected selectively from DEPC modification in the presence of excess Ni(II). However, it is important to note here that not all of the His48 residues are protected from reacting with DEPC in the presence of excess Ni(II); in the MS/MS analyses, a few DEPC-modified b fragment ions containing His48 are observed at very low intensities (Figure S9C). This result is expected given that only two of the four His48 residues per DNA-bound tetramer are positioned on the protein face oriented toward the DNA whereas the other two His48 residues are positioned on the opposite face of the repressor relative to the DNA, so it is possible that only two of the four residues participate in low-affinity Ni(II) binding. Together, these data identify unambiguously His48 as the residue in the tryptic peptide that is protected from DEPC modification by the presence of excess Ni(II). MS/MS analyses also confirmed that the degree of His123 and His125 modifications did not change in the presence of increasing concentrations of Ni(II) (data not shown). MS/MS analysis of the largest peptide containing residues 71−102, which includes all of the high-affinity Ni(II)-binding ligands, was complicated by the factors described above so it was not possible to pinpoint whether any specific residues were more protected in the presence of extra nickel. However, among the residues on this peptide, His92 is the most interesting because it is located on a surface loop facing His76−79 and Asp 80; together, these residues form a potential metal-binding site.

The Roles of H48, H92, H110, and H125 in the DNA-Binding Response to Low-Affinity Ni(II) Binding. Differential labeling of NikR in the presence of DNA and increasing concentrations of Ni(II) suggested that His48 and His110 may be involved in low-affinity Ni(II) binding. However, these experiments do not exclude the possibility that the protection observed in the presence of excess Ni(II) is due to a conformational change in the protein and not a direct result of metal−ligand coordination. It is also possible that carbethoxy groups were lost differentially during sample preparation prior to mass detection resulting in false identification of "protected" histidines. Therefore, to test independently whether His48 and His110 are required for low-affinity Ni(II) binding, single- and double-asparagine mutants of His48 and His110 were constructed. His125 was also mutated to asparagine as a negative control, to confirm that this residue is not involved in low-affinity Ni(II) binding. Finally, His92 was mutated to alanine to determine whether this residue, positioned adjacent to the HHHD sequence following His76 of the high-affinity Ni(II) site on the opposing monomer, contributes to low-affinity Ni(II)-induced DNA binding. Several experiments confirmed that these mutations did not affect either the secondary or quaternary structures (as reported by circular dichroism and size exclusion chromatography, respectively, Figure S5) or the high-affinity Ni(II)-binding properties (as determined by EGTA competition experiments, Figure S6).

The effect of these histidine mutations on the low-affinity Ni(II)-dependent DNA-binding activity was examined by MSA in the presence of 35 μM excess Ni(II). The concentration of wild-type NikR required for half-maximal DNA binding in the presence of excess Ni(II) is roughly 10 pM (Figures 3 and 6). Experiments with 10 pM protein revealed close to half-maximal DNA binding with H125N or H92A NikR in the presence of

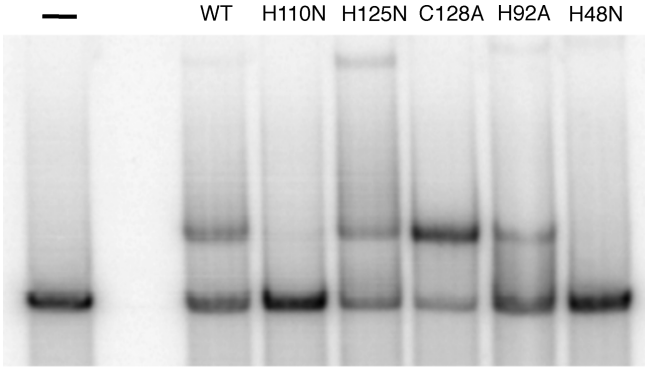

FIGURE 6: DNA binding of NikR and NikR mutants in the presence of excess Ni(II). NikR or the indicated NikR mutant protein (10 pM) was incubated with the 133-bp oligonucleotide containing the *nik* recognition sequence in the presence of 35 μM $NiSO_4$. The reactions were analyzed on a 7% native gel with 35 μM $NiSO_4$ in the gel and running buffer. No protein was added to the first lane.

excess Ni(II) (Figure 6 and Table 1), similar to wild-type protein. However, following incubation with 10 pM H48N or H110N NikR no DNA binding was observed (Figure 6), suggesting that the DNA-binding response to nickel is abrogated in these mutants.

The double mutant H48N/110N was then prepared and the DNA-binding activity examined. DNase footprinting experiments performed with the H48/110N mutant in the presence of stoichiometric Ni(II) produced a footprint at the binding site around the transcription start site similar to that of wild-type NikR and yielded K_D values of ~350 nM (Table 1, Figure 7), which is ~10× weaker than WT. A significantly more dramatic difference in the K_D of the protein−DNA complex is observed in the presence of excess Ni(II). The DNA affinity of the double mutant was sufficiently weak such that it could be measured by both MSA and DNase-footprinting experiments, revealing a K_D of ~15 nM in both types of assays (Table 1, Figure 7, and Figure S11). So the addition of excess nickel to the H48/110N holoprotein DNA complex results in only an ~20× tighter DNA affinity, compared to WT which exhibits an ~3000× stronger K_D for the DNA in the presence of excess Ni(II) compared to 1:1 Ni(II).

Finally, the high propensity of *E. coli* WT NikR to aggregate in the presence of more than stoichiometric amounts of Ni(II) in the absence of DNA has been observed previously and proposed to be evidence for the existence of low-affinity metal-responsive sites that participate in Ni(II)-induced aggregation (ref *46* and unpublished observations). Typically, a weak nickel competitor such as glycine is included in direct nickel titrations in order to minimize protein aggregation upon the addition of more than 1 equiv of nickel (*12*, *16*). Upon titration of apo-H48/110N with increasing amounts of nickel, a linear increase in absorbance at 302 nm was observed, yielding an ε_{302} value of $(7.3 \pm 0.3) \times 10^3$ M^{-1} cm^{-1}, analogous to WT (Figure S10). Unexpectedly, titration of H48/110N with Ni(II) beyond 1 equiv of Ni(II) in the absence of glycine did not result in protein aggregation, unlike wild type, confirming that the double mutant is more stable than WT in the presence of excess Ni(II) (Figure S10). These results suggest that the H48/110N mutations disrupt NikR's response to excess Ni(II). Taken together, these experiments reveal that the H110N and H48N mutations in NikR disrupt dramatically the low-affinity Ni(II) site(s) responsible for tight DNA binding and Ni(II)-induced precipitation but do not abrogate completely low-affinity Ni(II)-induced DNA binding.

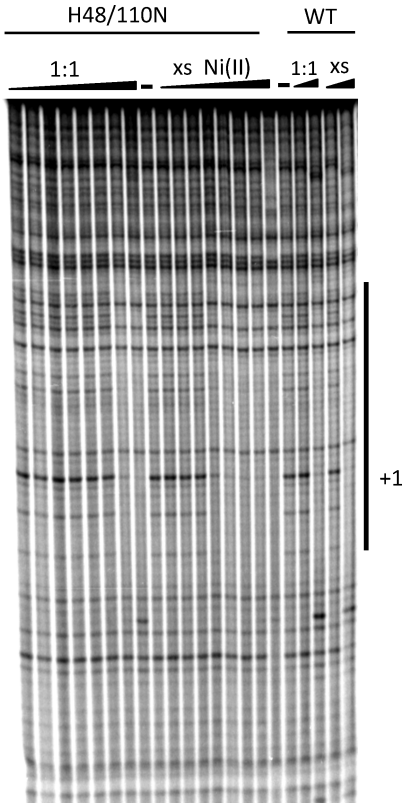

FIGURE 7: DNase footprinting of H48/110N in the presence of stoichiometric and excess Ni(II). Aliquots of H48/110N mutant (0.1, 1, 10, 25, 50, and 100 nM, 1, 10, and 0 μM) were incubated with stoichiometric Ni(II) (1:1) or 35 μM excess Ni(II) (xs) and with the 133-bp DNA probe containing the *nik* recognition sequence for 1 h at room temperature prior to the addition of DNase I and analysis on an 8% denaturing polyacrylamide gel. WT (0.1 nM and 1 μM) control DNase cutting reactions were performed under the same conditions as the mutant, in the presence of stoichiometric and excess Ni(II). Note that complete protection is not observed with 0.1 nM WT NikR in the presence of excess nickel because the DNA concentration is higher than the protein concentration. The transcription start site and area of protection are indicated.

DISCUSSION

Biochemical and *in vivo* experiments suggest that *E. coli* NikR mediates two levels of repression on the *nik* promoter in response to different Ni(II) concentrations. In the absence of Ni(II), no DNA binding is observed with up to ~2 μM protein by using either MSA or DNase footprinting assays. In the presence of stoichiometric Ni(II), NikR binds to the *nik* promoter with a nanomolar K_D (*15*, *18*). Although this NikR-DNA complex formed in the presence of stoichiometric Ni(II) is observed in DNase footprinting experiments, it is not detected by using the MSA (*12*, *18*). In contrast, in the presence of excess Ni(II) a significantly tighter NikR−DNA complex is observed in both DNase footprinting experiments as well as in MSAs run with metal in both the gel and the running buffer, and the K_D for the DNA complex decreases dramatically by 3 orders of magnitude from ~5 to 30 nM for the holoprotein complex to ~20 pM with excess nickel (*12*, *15*, *18*).

The observed increase in DNA-binding affinity in the presence of extra Ni(II) suggests either the existence of at least two distinct Ni(II)-binding sites or that there is only one metal-binding site on NikR that changes affinity upon formation of the complex with DNA. However, the XAS study, nickel release data, and chemical modification/mass spectrometry experiments presented

here indicate that the coordination sphere around the nickel in the high-affinity sites does not change significantly upon DNA binding, in agreement with previous structural analysis (*19*, *25*). These results thus support the hypothesis that there is a high-affinity Ni(II) site that is filled with stoichiometric metal and that it is distinct from one or more low-affinity Ni(II) site(s).

How nickel activates DNA binding by NikR is a question that remains to be resolved conclusively (*21*). The initial crystal structure of apo-NikR revealed a conformation of the tetrameric protein in which the two DNA-binding domains are facing in opposite directions (*14*), and it was reasonable to suggest that nickel binding causes the RHH motifs to swing down to the same face of the protein so that they can concurrently bind to the DNA recognition sequence without significant distortion of the double helix. However, this type of rearrangement was not observed in the structure of NikR loaded with stoichiometric nickel in the absence of DNA (*19*), and more subtle changes induced by the binding of the high-affinity nickel may be important for DNA binding (*19*, *21*). The structure of the Ni(II)−NikR−DNA complex revealed two ions at the interfaces between the DNA-binding domains and the tetrameric core of the protein (Figure 1), which were best modeled as potassium ions (*19*). These ions appear to be optimally placed to enhance the DNA-binding activity of NikR because they would reinforce the conformation of the protein with the DNA-binding domains in the *cis* orientation, and it was possible that they act as placeholders for the low-affinity nickel sites (*19*, *23*). However, molecular simulations indicate that potassium is preferred over nickel at this position (*20*), and recent biochemical analysis demonstrated that potassium is required for DNA binding by NikR loaded with either stoichiometric or extra nickel (*24*), suggesting that the low-affinity nickel site is in a location distinct from the potassium ions.

Previous studies demonstrated that metal-binding ligands can be mapped by using selective chemical modification followed by MS (*41*, *42*, *47*). Although many factors influence cysteine and histidine reactivities, including solvent accessibility, hydrogen bonding, and ionization state, it is reasonable to predict that the nucleophilicity of these groups will be diminished significantly upon the formation of metal complexes of sufficient thermodynamic stability due to slow rates of metal dissociation (*41*). This change is what is observed for both the high- and low-affinity Ni(II)-binding ligands of NikR. Our chemical modification experiments are based on the assumptions that (1) the low-affinity Ni(II) ions of NikR are filled in the presence of ~200 μM Ni(II) when the protein is bound to DNA and (2) Ni(II) coordination to the low-affinity site residues can protect the ligands from chemical modification. If the midnanomolar Ni(II)-binding affinity estimated for the low-affinity Ni(II) site is accurate (*18*), then the first assumption is reasonable given the micromolar protein concentrations used in these experiments. Furthermore, previous studies have demonstrated that the reactivities of cysteines and histidines in proteins that bind ligands with nanomolar affinities can be probed by sulfhydryl- and histidine-specific modifying agents (*48*, *49*). However, the presence of significantly weaker metal sites, such as those observed in the nickel soaks of the NikR−DNA complex crystals (*19*), cannot be excluded.

An examination of the crystal structures of *E. coli* NikR revealed multiple potential metal-binding sites on the protein in addition to the high-affinity nickel-binding sites, which is not surprising given that each NikR monomer contains 12 histidines and 2 cysteines as well as 16 aspartates/glutamates. Both of the Cys95 and Cys128 thiolates are chemically modified in apo-NikR. In the presence of 1 equiv of Ni(II), the high-affinity ligand Cys95 is protected significantly from chemical modification, consistent with the high thermodynamic stability of the Ni(II)−NikR complex ($K_D \sim 1 \times 10^{-12}$ M) (*15*, *16*). The reactivity of Cys128, even in the presence of excess Ni(II) and DNA, indicated that this cysteine is not involved in the low-affinity Ni(II)-binding activity. This conclusion was confirmed by mutagenesis studies because the DNA-binding activity of the C128A mutant in the presence of excess nickel was only severalfold weaker than that of the wild-type protein. Cys128, His123′, and His125′ compose a cluster of metal-binding residues that appear to be suitably located to bind a Ni(II) ion at the interface with the DNA-binding domain; however, these experiments also demonstrated that substitution of His125 did not affect the low-affinity Ni(II)-induced DNA-binding response of NikR. Another potential metal-binding site, composed of the HHHHD sequence following His76 of the high-affinity site on a surface loop close to His92′ of the opposing monomer, was examined by mutating His92. This residue was of particular interest because the corresponding residue in *H. pylori* NikR, Glu104, serves as a ligand of a secondary nickel site (*26*). However, removing this modification did not appear to affect DNA binding in the presence of excess Ni(II), suggesting that this residue is also not involved in the response to low-affinity Ni(II) binding.

In contrast, the observation that His48 and His110 are protected significantly from DEPC modification only in the presence of excess Ni(II) and DNA suggests that these two histidines are involved in the DNA-binding response to the low-affinity Ni(II). Mutation of both of these histidines to noncoordinating residues selectively reduced the affinity of the NikR−DNA complex formed in the presence of excess Ni(II) compared to a much smaller effect on the K_D of the DNA complex formed upon loading stoichiometric Ni(II). Although substitutions of His48 and His110 do not disrupt completely the increase in affinity of the protein−DNA complex upon addition of excess nickel, the H48/110N mutant's response to excess Ni(II) compared to holoprotein is ~150× smaller than that of WT, resulting in a complex with a 1500-fold weaker affinity and indicating that the low-affinity Ni(II) site has been severely compromised. Furthermore, the observation that the double histidine mutation also slightly weakens the DNA interaction in response to stoichiometric nickel suggests that these residues may participate in the protein's response to loading the high-affinity site as well.

His48 is positioned on the linker connecting the metal-binding domain to the DNA-binding domain, and His110 is positioned on helix α4 on the surface of the metal-binding domain that faces the DNA-binding domain (Figure 1). It is not surprising given their exposed, solvent-accessible positions on the protein that both of these residues are highly susceptible to chemical modification. Moreover, the solvent accessibilities of His48 and His110 do not appear to change in a comparison of the structures of the DNA-bound and DNA-free holo-NikR complexes; therefore, we would not expect His48/110 to be protected due to the conformational change that occurs upon DNA binding of the protein loaded with stoichiometric nickel. Instead, the chemical modification/mass spectrometry results reveal that both His48 and His110 are protected by the addition of excess Ni(II) and DNA. These residues colocalize to the same region of the protein in the structure of the NikR−DNA complex, separated by Cα distances of ~10 Å. Ni(II) coordination to both His48 and

His110 would effectively position the metal ion between the metal- and DNA-binding domains. Furthermore, there are several carboxylate ligands in the vicinity of His48 and His110, including Asp104, Asp107, Asp113, and Asp114, which are good candidates for additional Ni(II) ligands because the distances between the side chains of His110 or His48 and any one of these aspartates are <7 Å. The carboxylate residue Glu43 is also positioned on the flexible linker, and metal coordination between His48, His110, and Glu43 or any of the aspartates listed above would likely pull helix α2 of the RHH domain closer to the metal-binding domain. As mentioned above, XAS of the nickel ion bound in the low-affinity site revealed an octahedral geometry coordinated by six N/O donors including two imidazoles (*25*), consistent with our results.

Analogous to the structural role of the K^+ ions (*19*, *24*), Ni(II) binding to the low-affinity Ni(II) sites might fix the relative orientations of the two domains in an active, tighter DNA-binding conformation. Additionally, His48 is positioned on the linker connected to helix α2 that must unwind partially to allow both DNA-binding domains to rotate to the same face of the protein upon binding the *nik* operator (Figure 1). Thus, Ni(II) binding between the interdomain hinge and the tetrameric core could buttress the tertiary structure of the protein upon unwinding of helix α2 and restrict interdomain mobility, thereby strengthening a conformation that allows the RHH motifs to make base-specific contacts with the DNA. Furthermore, Ni(II) binding to His48 and His110 could modulate helix α2, which was highlighted by Schreiter et al. as a likely component of signal propagation from the metal-binding domain to the RHH domain because of the high degree of sequence conservation in this helix (*14*).

A model of metal-activated DNA binding by *E. coli* NikR includes the three types of metal-binding sites discussed here (*21*). Nickel ions bind first to the four high-affinity sites in the middle of the protein tetramer, triggering conformational changes that result in nonspecific DNA binding. The potassium ions then provide support for the appropriate orientation of the DNA-binding domains, so that the protein can bind specifically to the *nik* promoter. Additional nickel binding generates a tighter DNA complex in a nickel-selective maner. In this study, classical chemical modification combined with mass spectrometric peptide mapping has been used as a sensitive approach for the direct identification of cysteine and histidine residues in both the high- and the low-affinity Ni(II) sites of *E. coli* NikR, and the locations of these residues are consistent with their roles as critical ligands in the allosteric metalloregulation of operator/promoter binding. The cytoplasmic source of nickel for these sites and how they relate to the other nickel proteins and pathways in *E. coli* remain to be addressed.

ACKNOWLEDGMENT

We thank Alistair Dias for XAS data collection. Portions of this research were carried out at the Stanford Synchrotron Radiation Lightsource, a national user facility operated by Stanford University on behalf of the U.S. Department of Energy, Office of Basic Energy Sciences. We thank Alex Young for ESI mass spectrometry data collection and advice. We also thank Michael Leach for a critical reading of the manuscript and members of the Zamble laboratory for helpful discussions.

SUPPORTING INFORMATION AVAILABLE

Table S1 containing the sequences of PCR primer for mutagenesis as well as the 54-bp oligonucleotide containing the *nik* recognition sequence, Figure S1 presenting XAS data of the high-affinity Ni(II) site in the presence and absence of DNA, Figure S2 showing a nickel release experiment, Figure S3 showing the chemical modification reactions used and Figure S4 showing the MS spectra following carboxamidomethylation of NikR in the absence of DNA, Figures S5 and S6 presenting the CD, GFC, and EGTA nickel competitions of WT and mutant NikR proteins, Figure S7 presenting the DNase footprinting of holo-C128A NikR, Figure S8 presenting the MS spectra following carboethoxylation of NikR and Figure S9 presenting the representative MS/MS data of peptide 38−65, and Figures S10 and S11 presenting nickel titration and the mobility shift assay data of H48/110N, respectively. This material is available free of charge via the Internet at http://pubs.acs.org.

REFERENCES

1. Ma, Z., Jacobsen, F. E., and Giedroc, D. P. (2009) Coordination chemistry of bacterial metal transport and sensing. *Chem. Rev. 109*, 4644–4681.
2. O'Halloran, T. V. (1993) Transition metals in control of gene expression. *Science 261*, 715–725.
3. Pennella, M. A., and Giedroc, D. P. (2005) Structural determinants of metal selectivity in prokaryotic metal-responsive transcriptional regulators. *BioMetals 18*, 413–428.
4. Waldron, K. J., and Robinson, N. J. (2009) How do bacterial cells ensure that metalloproteins get the correct metal? *Nat. Rev. Microbiol. 7*, 25–35.
5. De Pina, K., Desjardin, V., Mandrand-Berthelot, M. A., Giordano, G., and Wu, L. F. (1999) Isolation and characterization of the nikR gene encoding a nickel-responsive regulator in *Escherichia coli*. *J. Bacteriol. 181*, 670–674.
6. Dosanjh, N. S., and Michel, S. L. J. (2006) Microbial nickel metalloregulation: NikRs for nickel ions. *Curr. Opin. Chem. Biol. 10*, 123–130.
7. Li, Y., and Zamble, D. B. (2009) Nickel homeostasis and nickel regulation: An overview. *Chem. Rev. 109*, 4617–4643.
8. Chivers, P. T., and Sauer, R. T. (1999) NikR is a ribbon-helix-helix DNA-binding protein. *Protein Sci. 8*, 2494–2500.
9. Schreiter, E. R., and Drennan, C. L. (2007) Ribbon-helix-helix transcription factors: Variations on a theme. *Nat. Rev. Microbiol. 5*, 710–720.
10. Phillips, S. E. V. (1994) The β-ribbon DNA recognition motif. *Annu. Rev. Biophys. Biomol. Struct. 23*, 671–701.
11. Navarro, C., Wu, L.-F., and Mandrand-Berthelot, M.-A. (1993) The nik operon of *Escherichia coli* encodes a periplasmic binding-protein-dependent transport system for nickel. *Mol. Microbiol. 9*, 1181–1191.
12. Chivers, P. T., and Sauer, R. T. (2000) Regulation of high affinity nickel uptake in bacteria. Ni^{2+}-dependent interaction of NikR with wild-type and mutant operator sites. *J. Biol. Chem. 275*, 19735–19741.
13. Rowe, J. L., Starnes, G. L., and Chivers, P. T. (2005) Complex transcriptional control links NikABCDE-dependent nickel transport with hydrogenase expression in *Escherichia coli*. *J. Bacteriol. 187*, 6317–6323.
14. Schreiter, E. R., Sintchak, M. D., Guo, Y., Chivers, P. T., Sauer, R. T., and Drennan, C. L. (2003) Crystal structure of the nickel-responsive transcription factor NikR. *Nat. Struct. Biol. 10*, 794–799.
15. Chivers, P. T., and Sauer, R. T. (2002) NikR repressor: High-affinity nickel binding to the C-terminal domain regulates binding to operator DNA. *Chem. Biol. 9*, 1141–1148.
16. Wang, S. C., Dias, A. V., Bloom, S. L., and Zamble, D. B. (2004) Selectivity of metal binding and metal-induced stability of *Escherichia coli* NikR. *Biochemistry 43*, 10018–10028.
17. Diederix, R. E. M., Fauquant, C., Rodrigue, A., Mandrand-Berthelot, M. A., and Michaud-Soret, I. (2008) Sub-micromolar affinity of *Escherichia coli* NikR for Ni(II). *Chem. Commun.*, 1813–1815.
18. Bloom, S. L., and Zamble, D. B. (2004) Metal-selective DNA-binding response of *Escherichia coli* NikR. *Biochemistry 43*, 10029–10038.
19. Schreiter, E. R., Wang, S. C., Zamble, D. B., and Drennan, C. L. (2006) NikR-operator complex structure and the mechanism of repressor activation by metal ions. *Proc. Natl. Acad. Sci. U.S.A. 103*, 13676–13681.
20. Phillips, C. M., Nerenberg, P. S., Drennan, C. L., and Stultz, C. M. (2009) Physical basis of metal-binding specificity in *Escherichia coli* NikR. *J. Am. Chem. Soc. 131*, 10220–10228.

21. Wang, S. C., Dias, A. V., and Zamble, D. B. (2009) The "metallo-specific" response of proteins: A perspective based on the *Escherichia coli* transcriptional regulator NikR. *Dalton Trans*. 2459–2466.
22. Outten, C. E., and O'Halloran, T. V. (2001) Femtomolar sensitivity of metalloregulatory proteins controlling zinc homeostasis. *Science 292*, 2488–2492.
23. Chivers, P. T., and Tahirov, T. H. (2005) Structure of *Pyrococcus horikoshii* NikR: Nickel sensing and implications for the regulation of DNA recognition. *J. Mol. Biol. 348*, 597–607.
24. Wang, S. C., Li, Y., Robinson, C. V., and Zamble, D. B. (2010) Potassium is critical for the Ni(II)-responsive DNA-binding activity of *Escherichia coli* NikR. *J. Am. Chem. Soc. 132*, 1506–1507.
25. Leitch, S., Bradley, M. J., Rowe, J. L., Chivers, P. T., and Maroney, M. J. (2007) Nickel-specific response in the transcriptional regulator, *Escherichia coli* NikR. *J. Am. Chem. Soc. 129*, 5085–5095.
26. Dian, C., Schauer, K., Kapp, U., McSweeney, S. M., Labigne, A., and Terradot, L. (2006) Structural basis of the nickel response in *Helicobacter pylori*: Crystal structures of HpNikR in apo and nickel-bound states. *J. Mol. Biol. 361*, 715–730.
27. Bahlawane, C., Dian, C., Muller, C., Round, A., Fauquant, C., Schauer, K., de Reuse, H., Terradot, L., and Michaud-Soret, I. (2010) Structural and mechanistic insights into *Helicobacter pylori* NikR activation. *Nucleic Acids Res. 38*, 3106–3118.
28. Abraham, L. O., Li, Y., and Zamble, D. B. (2006) The metal- and DNA-binding activities of *Helicobacter pylori* NikR. *J. Inorg. Biochem. 100*, 1005–1014.
29. Benanti, E. L., and Chivers, P. T. (2007) The N-terminal arm of the *Helicobacter pylori* Ni^{2+}-dependent transcription factor NikR is required for specific DNA binding. *J. Biol. Chem. 282*, 20365–20375.
30. Delany, I., Ieva, R., Soragni, A., Hilleringmann, M., Rappuoli, R., and Scarlato, V. (2005) In vitro analysis of protein-operator interactions of the NikR and Fur metal-responsive regulators of coregulated genes in *Helicobacter pylori*. *J. Bacteriol. 187*, 7703–7715.
31. Dosanjh, N. S., Hammerbacher, N. A., and Michel, S. L. J. (2007) Characterization of the *Helicobacter pylori* NikR-PureA DNA Interaction: Metal ion requirements and sequence specificity. *Biochemistry 46*, 2520–2529.
32. Zambelli, B., Danielli, A., Romagnoli, S., Neyroz, P., Ciurli, S., and Scarlato, V. (2008) High-affinity Ni^{2+} binding selectively promotes binding of *Helicobacter pylori* NikR to its target urease promoter. *J. Mol. Biol. 383*, 1129–1143.
33. Li, Y., and Zamble, D. B. (2009) pH-responsive DNA-binding activity of *Helicobacter pylori* NikR. *Biochemistry 48*, 2486–2496.
34. Lundblad, R. L., and Noyes, C. M. (1984) Chemical Reagents for Protein Modification, pp 101−125, CRC Press, Boca Raton, FL.
35. Hunt, J. B., Neece, S. H., and Ginsburg, A. (1985) The use of 4-(2-pyridylazo)resorcinol in studies of zinc release from *Escherichia coli* aspartate transcarbamoylase. *Anal. Biochem. 146*, 150–157.
36. Leach, M. R., Sandal, S., Sun, H., and Zamble, D. B. (2005) The metal-binding activity of the *Escherichia coli* hydrogenase maturation factor HypB. *Biochemistry 44*, 12229–12238.
37. Dias, A. V., Mulvihill, C. M., Leach, M. R., Pickering, I. J., George, G. N., and Zamble, D. B. (2008) Structural and biological analysis of the metal sites of *Escherichia coli* hydrogenase accessory protein HypB. *Biochemistry 47*, 11981–11991.
38. Helmann, J. D. (2002) Sensing nickel: NikRs with two pockets. *Chem. Biol. 9*, 1055–1057.
39. Carrington, P. E., Chivers, P. T., Al-Mjeni, F., Sauer, R. T., and Maroney, M. J. (2003) Nickel coordination is regulated by the DNA-bound state of NikR. *Nat. Struct. Biol. 10*, 126–130.
40. Colpas, G. J., Maroney, M. J., Bagyinka, C., Kumar, M., Willis, W. S., Suib, S. L., Baidya, N., and Mascharak, P. K. (1991) X-ray spectroscopic studies of nickel complexes, with application to the structure of nickel sites in hydrogenases. *Inorg. Chem. 30*, 920–928.
41. Apuy, J. L., Busenlehner, L. S., Russell, D. H., and Giedroc, D. P. (2004) Ratiometric pulsed alkylation mass spectrometry as a probe of thiolate reactivity in different metalloderivatives of *Staphylococcus aureus* pI258 CadC. *Biochemistry 43*, 3824–3834.
42. Gonzalez De Peredo, A., Saint-Pierre, C., Adrait, A., Jacquamet, L., Latour, J. M., Michaud-Soret, I., and Forest, E. (1999) Identification of the two zinc-bound cysteines in the ferric uptake regulation protein from *Escherichia coli*: Chemical modification and mass spectrometry analysis. *Biochemistry 38*, 8582–8589.
43. Miles, E. W. (1977) Modification of histidyl residues in proteins by diethylpyrocarbonate. *Methods Enzymol. 47*, 431–442.
44. Ehrenberg, L., Fedorcsak, I., and Solymosy, F. (1976) Diethyl pyrocarbonate in nucleic acid research. *Prog. Nucleic Acid Res. Mol. Biol. 16*, 189–262.
45. Oberg, B. (1971) Carbethoxylation of polynucleotides. *Eur. J. Biochem. 19*, 496–501.
46. Fauquant, C., Diederix, R. E. M., Rodrigue, A., Dian, C., Kapp, U., Terradot, L., Mandrand-Berthelot, M. A., and Michaud-Soret, I. (2006) pH dependent Ni(II) binding and aggregation of *Escherichia coli* and *Helicobacter pylori* NikR. *Biochimie 88*, 1693–1705.
47. Qin, K., Yang, Y., Mastrangelo, P., and Westaway, D. (2002) Mapping Cu(II) binding sites in prion proteins by diethyl pyrocarbonate modifications and matrix-assisted laser desorption ionization-time of flight (MALDI-TOF) mass spectrometric footprinting. *J. Biol. Chem. 277*, 1981–1990.
48. Silverman, J. A., and Harbury, P. B. (2002) Rapid mapping of protein structure, interactions, and ligand binding by misincorporation proton-alkyl exchange. *J. Biol. Chem. 277*, 30968–30975.
49. Weng, L. X., Xu, J. L., Li, Q., Birch, R. G., and Zhang, L. H. (2003) Identification of the essential histidine residue for high-affinity binding of AlbA protein to albicidin antibiotics. *Microbiology 149*, 451–457.